

# Exotica and the Confining Flux

J. Kuti<sup>a</sup>

<sup>a</sup>Department of Physics, University of California at San Diego, La Jolla, California 92093-0319

Recent developments in Quantum Chromodynamics (QCD) are reviewed on three major topics where nonperturbative gluon excitations of the QCD vacuum and the physical properties of the confining flux play a central role: (1) New lattice results on the spectrum and wave functions of heavy  $Q\bar{Q}$ gluon molecules, known as heavy hybrids, will be discussed. (2) Recent advances on the glueball spectrum in lattice QCD will be presented with some theoretical observations. (3) Progress in our understanding of the nonperturbative internal structure of the confining flux and its excitation spectrum will be reported.

## INTRODUCTION AND OUTLINE

I will review here three topics with considerable progress in phenomenologically relevant and theoretically challenging areas of lattice QCD. They are all related to nonperturbative gluon excitations of the QCD vacuum and the physical properties of the confining flux. The limited scope of the talk does not include discussions on some exotic objects, like light hybrids [1,2] and dibaryons [3], or glueball phenomenology [1,4], and some other topics which were reviewed, or presented elsewhere at the conference. The outline of the talk is as follows:

1. *Heavy Hybrid Spectrum*
  - Methods and Phenomenology
  - Born-Oppenheimer Approximation
  - NRQCD Hybrid Spectrum
  - Results from the MILC Collaboration
2. *Glueball Spectrum*
  - Review of Recent Lattice Results
  - Composite Glueball Operators
  - Constituent Gluon Model
3. *The Confining Flux*
  - Microscopic Vacuum Model
  - Casimir Scaling and Multiple Sources
  - Where Is the String Limit?
  - Flux Fission (String Breaking)

The chromoelectric flux with static sources is the organizing theme of the selected topics. Its ground state energy explains the origin of the confining potential of heavy  $Q\bar{Q}$  pairs. The excitation spectrum of the confining (and confined)

flux defines hybrid  $Q\bar{Q}$  potentials which bind quark-antiquark pairs into heavy hybrid  $Q\bar{Q}$ gluon molecules. Higher excited flux states are unstable against glueball emission requiring a detailed study of the glueball spectrum. The confined flux, when stretched, is expected to reach the limiting behavior of an effective QCD string in geometric string variables which remains a topic of considerable theoretical interest. The stretched flux can also fission by quark-antiquark pair creation in the QCD vacuum with important phenomenological implications. Flux states with sources in higher color representations, or with multiple color sources, like three-quark and four-quark configurations, provide further information on flux formation in the confining vacuum.

## 1. HEAVY HYBRID SPECTRUM

I will review recent results on the heavy hybrid spectrum from three complementary approaches, followed by a brief phenomenological note.

### Methods and Phenomenology

The first method is based on the Born-Oppenheimer expansion. In this approach, the heavy hybrid meson is treated analogous to a diatomic molecule: the slow heavy quarks correspond to the nuclei and the fast gluon field corresponds to the electrons [5,6]. The first step in the Born-Oppenheimer treatment is to determine the energy levels of the glue (and light quark-antiquark pairs) as a function of the heavy quark-antiquark separation, treating the heavy

quark and antiquark simply as spatially-fixed color sources. Each such energy level defines an adiabatic potential. The quark motion is then restored by solving the nonrelativistic Schrödinger equation using these potentials. Conventional quarkonia arise from the lowest-lying potential; hybrid quarkonium states emerge from the excited potentials. The leading Schrödinger kinetic energy term and the omission of retarded transverse gluons (in Coulomb gauge), radiated and reabsorbed by the slowly moving quarks, could be corrected in a systematic expansion.

The starting point of the second method is the lattice formulation of the euclidean NRQCD framework with the heavy quark propagating according to a spin-independent nonrelativistic action [7]. Retarded gluon effects are included, spin effects and corrections to the leading kinetic term can be also added without difficulty. I will report new NRQCD results which show that gluon retardation effects are very small in the bottomonium system and its hybrid excitations confirming the success of the leading Born-Oppenheimer approximation.

The third approach which was explored by the MILC collaboration [8] applies Wilson and clover lattice fermions in the mass range of the charmed quark to explore the hybrid excitations of the charmonium system. The heavy  $c$  quark is treated without nonrelativistic approximation and all spin and retardation effects are included.

I should note that the phenomenology of heavy hybrids is very interesting. Early results from the CUSB and CLEO collaborations [9,10] revealed a complex resonance structure between the  $b\bar{b}$  threshold and 11.2 GeV in  $e^+e^-$  annihilation as shown in Fig.1. This is precisely the energy range where the lowest hybrid excitations are expected. Today it would only take a very short run for the upgraded CLEO detector to rescan this region with much higher resolution to find perhaps, for the first time, gluon excitations in the hadron spectrum under experimentally and theoretically rather well-controlled circumstances. This is an exciting area where lattice work will remain the dominant method.

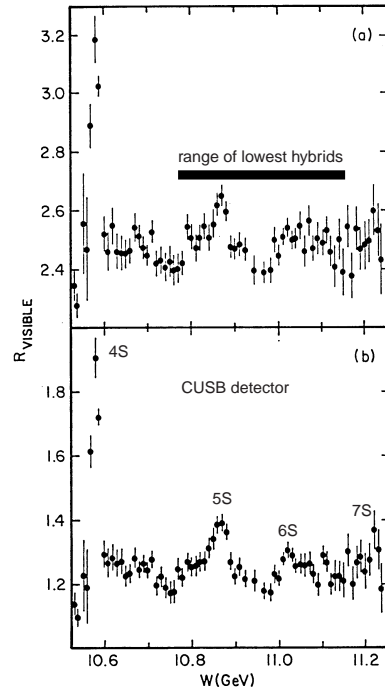


Figure 1. The CUSB scan of the energy region above the  $b\bar{b}$  threshold is shown [9] together with the expected mass range of the lowest heavy hybrid  $b\bar{b}$ gluon states. The conventional interpretation of the resonance peaks corresponds to the radial excitations of the  $\Upsilon$  particle [11].

### Born-Oppenheimer Approximation

The lowest hybrid potential which is depicted in Fig.2 corresponds to a gluon excitation with one unit of angular momentum projected along the quark-antiquark (molecular) axis with  $CP = -1$  quantum numbers (excited  $\Pi_u$  state above the  $\Sigma_g^+$  ground state in spectroscopic notation). I will discuss the full spectrum of gluon excitations in Section 3. Following Ref. [16], the physical scale  $r_0$  in Fig.2 is defined by the relation  $[r^2 dV_{\Sigma_g^+}(\vec{r})/dr]_{r=r_0} = 1.65$ .

An important recent study [17] shows in Fig.3 that dynamical quark loop effects are not visible at larger distances, out to 1.2 fm separation of the quark-antiquark pair in the  $\Sigma_g^+$  and  $\Pi_u$  potentials. This further supports the accuracy and

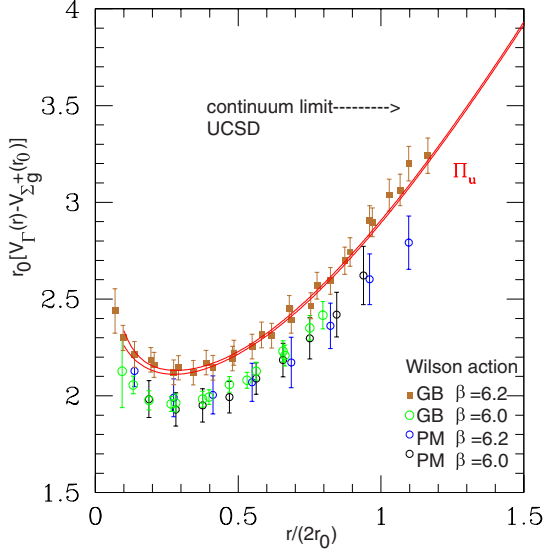


Figure 2. Results from mean-field improved anisotropic lattice actions [12,13] are compared to recent [14](GB) and earlier [15](PM) simulations with Wilson actions. The excited hybrid potential has quantum numbers  $\Gamma = \Pi_u$ . Consistency across Refs. [12–14] is excellent for small Wilson gauge coupling.

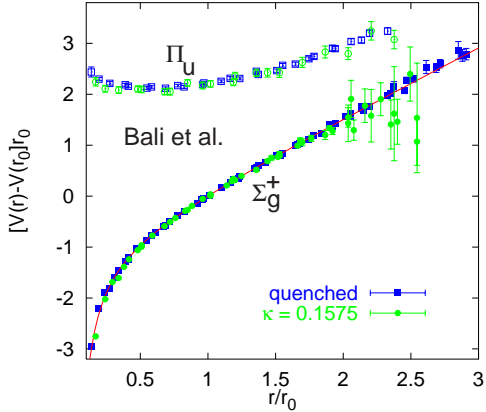


Figure 3. Wilson quark loop effects are shown for the light quark mass range where  $m_\pi \sim m_\rho/2$  [17].

phenomenological relevance of the approach.

The spectra of heavy hybrid states built on the two lowest hybrid potentials  $V_{\Pi_u}(\vec{r})$  and  $V_{\Sigma_u^-}(\vec{r})$  are shown in Fig.4. The most prominent fea-

ture of the spectrum is the dense set of radial excitations in the rather shallow hybrid potentials with level separations  $\sim 200 - 300$  MeV. The hybrid wavefunctions all vanish at the origin

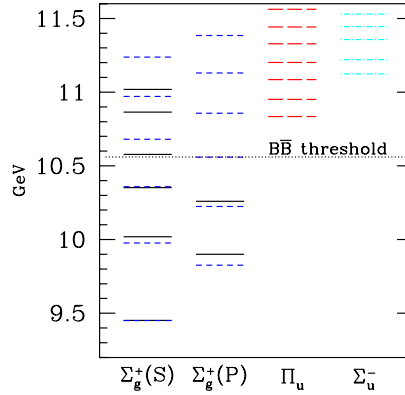


Figure 4. The Schrödinger spectrum of the adiabatic hybrid potentials is shown in comparison with the conventional S and P states of the  $b\bar{b}$  spectrum.

due to the repulsive Coulomb core in the potential and the special centrifugal term in the adiabatic Schrödinger equation [5,6]. The hybrid Schrödinger states are also much more extended than the conventional quark-antiquark states, as depicted in Fig.5.

Once the hybrid potentials are determined, the Born-Oppenheimer approach yields the entire leading-order spectrum, in contrast to direct NRQCD simulations. However, the validity of the Born-Oppenheimer approximation relies on the smallness of retardation effects. In addition, spin-dependent corrections have to be included for precise predictions. Quantitative estimates on retardation effects comes from direct comparison of mass splittings in the leading Born-Oppenheimer approximation with those determined from NRQCD simulations.

### NRQCD Hybrid Spectrum

Recent results on heavy hybrid states were reported using anisotropic coarse lattices with mean-field improved action [12,13], and Wilson

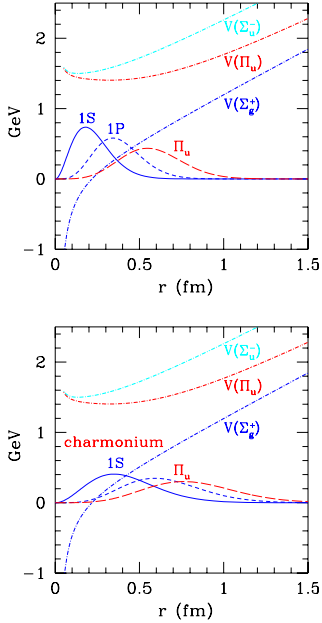


Figure 5. The radial probability distribution in the lowest  $\Pi_u$  hybrid state is shown in comparison with conventional  $b\bar{b}$  S and P states of the bottomonium (upper box) and charmonium system.

gauge action [18,19]. In Ref. [13] the bare quark mass was taken to be  $a_s M_b = 2.56$ . The so-called kinetic mass of the  $\Upsilon$  was then determined from its low-momentum dispersion relation. Half of this mass was used for the quark mass in the leading Born-Oppenheimer calculation. This ensured that the  $\Upsilon$  kinetic masses were identical in both calculations. A typical effective mass plot for hybrid states from the NRCQD run with improved action on asymmetric lattices is shown in Fig.6 [13]. The hybrid mass with Wilson gauge action [18] was found noticeably higher, but part of the disagreement might be attributable to the different choice of setting the physical scale. Results from Ref. [13] are consistent with earlier work [12,19] adding improved control on systematics and statistics. One of the new features here is the clear signal for the first radial hybrid excitation. The statistical error on the mass of the

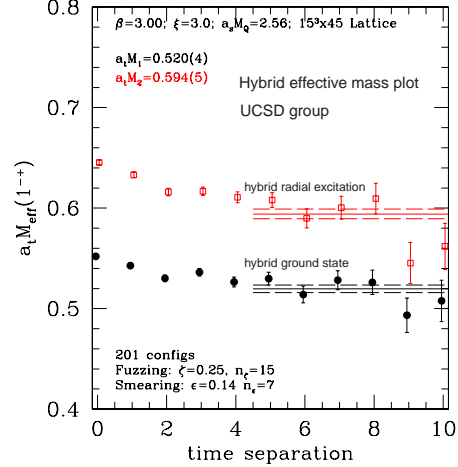


Figure 6. Mass estimates are shown for the lowest hybrid  $\Pi_u$  state and its first radial excitation [13].

hybrid  $b\bar{b}g$  state is small but the systematic study of lattice artifacts remains incomplete. Assuming small lattice artifacts in the simulation results, it was shown that gluon retardation affects the spin-averaged mass splittings by less than ten percent, validating the leading Born-Oppenheimer approximation [13].

## Results from the MILC Collaboration

The MILC collaboration repeated its original Wilson simulations of the hybrid meson spectrum [20] using the clover action [8]. The new results, shown in Fig.7 for the  $1^{-+}$  heavy hybrid mass, are consistent with earlier MILC Wilson runs providing an important check on charmed quark lattice artifacts. Preliminary results for the wave function of the  $1^{-+}$  state in Coulomb gauge were also reported at the conference [8].

## 2. GLUEBALL SPECTRUM

In the perspective of ten years it is quite remarkable how much is known now about the quenched glueball spectrum. Hopefully, it will not take another ten years before quark-antiquark vacuum polarization effects are included systematically, with control comparable to the quenched results.

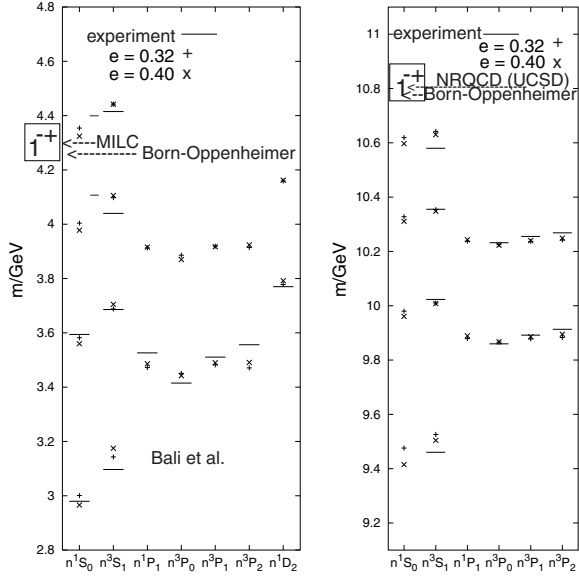


Figure 7. The lowest hybrid states are shown in the charmonium and bottomonium spectrum from three different methods described in the text. The spin-dependent potential model spectrum is superimposed for comparison from Ref. [21] where the notation is explained.

### Review of Recent Lattice Results

The construction of improved anisotropic lattice actions using mean-field improved perturbation theory is discussed in Ref. [22] with further pointers to the literature. All recent results reviewed here are based on this action which was designed to be  $O(a_s^2)$  improved and to include terms that directly couple links only on adjacent time slices to avoid spurious modes in the gluon propagator. The hadronic scale parameter  $r_0$ , defined earlier, is used in the conversion of the measured glueball masses into physical units. The method has been applied to the SU(3) glueball spectrum by Morningstar and Peardon [22] whose comprehensive lattice spin analysis [23,24] is shown in Fig.8. Recently a detailed analysis of the SU(2) glueball spectrum using very similar methods was also presented [25]. The assignment of continuum spin labels to lattice states in Fig.8 is based on transformation properties of the glueball states under the cubic

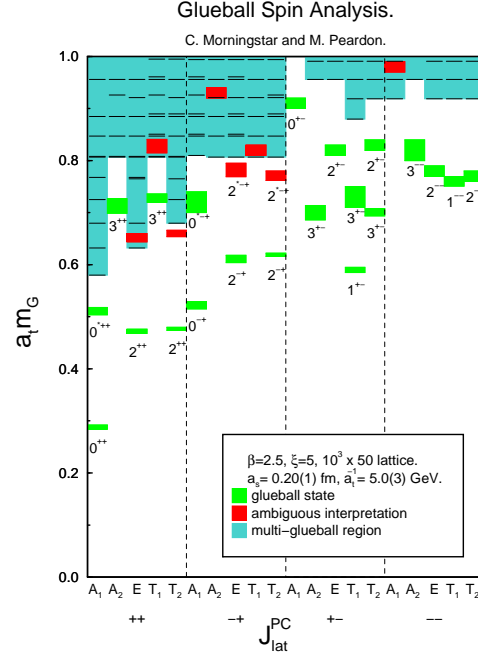


Figure 8. The SU(3) lattice spectrum of glueball states in the quenched approximation.

point group, combined with parity and charge conjugation operations [22,24]. The continuum spin quantum numbers are not always fully resolved across cubic group representations (designated as ambiguous states). The bottom of the shaded area in each channel of Fig.8 indicates where the continuum threshold of the lightest two-glueball state is located. Glueball states above the continuum threshold are not included in the final spin analysis of the continuum spectrum in Fig.9. The two lightest glueballs, the scalar and tensor, have candidate resonances [27–29]: the  $f_0(1500)$  and  $f_J(1710)$  scalar states and the  $\xi(2230)$  tensor candidate. Both  $f_0(1500)$  and  $f_J(1710)$  are consistent with lattice mass predictions in the pure-gauge theory [26,30,22] of 1600 MeV with systematic errors of approximately 100 MeV. The glueball spectrum from the Wilson action is shown in Fig.10, together with the spectrum from a constituent gluon model.

The SESAM collaboration [31] has investigated the scalar and tensor glueballs on their large en-

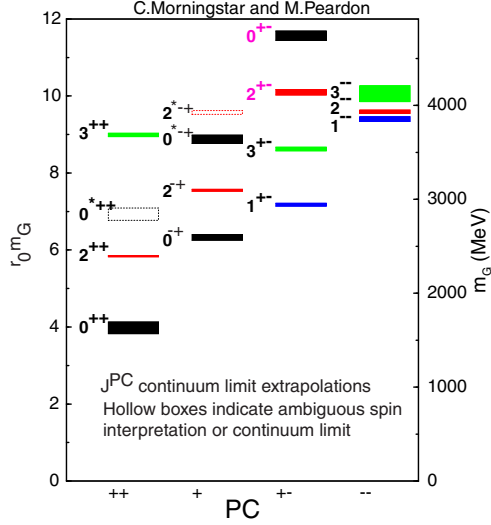


Figure 9. Final spin analysis of the continuum glueball spectrum.

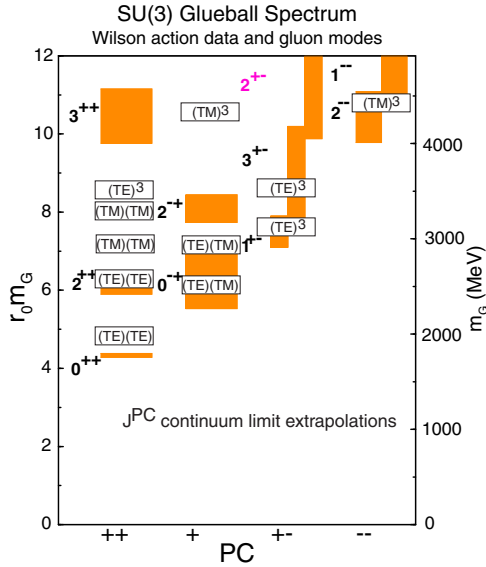


Figure 10. The range of energy levels from several Wilson action runs is indicated by shaded areas. The constituent gluon spectrum (discussed in the text) is also displayed with the occupied gluon modes.

semble of unquenched (Wilson gauge and quark action) configurations. Only little change has been found in the masses of these states as the sea quark mass runs down from the strange quark mass to  $(m_\pi/m_\rho \approx 0.5)$  but enhanced finite-volume dependence was noticed which is perhaps attributable to dynamical quark effects.

### Composite Glueball Operators

In a confining theory it is difficult to relate physical glueball states to fundamental gluon fields. There is, however, a qualitative expectation that higher dimensional interpolating operators will create higher mass states [32–34]. This rule works well for light mesons and baryons and now I will apply it to the glueball spectrum.

Local composite operators of the gluon field act as interpolating fields for glueball states. For example, the state with  $0^{-+}$  quantum numbers is created from the physical vacuum by the operator  $\vec{E}_a \cdot \vec{B}_a$  ( $a=1,2,\dots,8$  stands for color summation) so that  $\langle 0^{-+} | \vec{E}_a \cdot \vec{B}_a | \text{vacuum} \rangle \neq 0$ . It is not difficult to determine the quantum numbers of all the glueball states which are generated by the lowest dimensional ( $\text{dim}=4,5,6$ ) operators. A small representative sample is listed in Table 1.

Table 1

Sample of  $\text{dim}=4,6$  operators which create various  $J^{PC}$  quantum numbers.

dimension	$J^{PC}$	Operator
4	$0^{-+}$	$\vec{E}_a \cdot \vec{B}_a$
4	$0^{++}$	$\vec{E}_a^2 - \vec{B}_a^2$
4	$2^{++}$	$\vec{E}_a^i \vec{E}_a^j + \vec{B}_a^i \vec{B}_a^j - \frac{1}{3} \delta^{ij} (\vec{E}_a^2 + \vec{B}_a^2)$
6	$0^{-+}$	$f_{abc} (\vec{E}_a \times \vec{E}_b) \cdot \vec{E}_c$
6	$1^{-+}$	$f_{abc} (\vec{B}_a \cdot \vec{E}_b) \vec{B}_c$
6	$2^{-+}$	$f_{abc} (\vec{E}_a \times \vec{E}_b)^i \vec{E}_c^j + \dots$

In classifying the lowest glueball excitations according to their quantum numbers, Morningstar and Peardon report 15+5 states where the last five are labelled as questionable. The lowest dimensional operators with  $\text{dim}=4,5,6$  create states whose quantum numbers match onto the observed spectrum nearly perfectly. This is quite remarkable, given the simplicity of the argument.

## Constituent Gluon Model

The notion of constituent gluons stems from the general idea of quasi-particles in some effective QCD mean field theory of hadrons. In such a description the fundamental gluon field is replaced by Hartree modes of some constituent gluon field with residual perturbative interactions inside glueballs. It is hoped, for example, that the  $1/N$  expansion might eventually lead to a similar Hartree picture. I will identify the Hartree states with free gluon modes in a bubble (bag) with confining boundary conditions [35,36]. Admittedly speculative, the model in its simplest form leads to detailed predictions on the glueball spectrum.

We will picture the QCD vacuum as a dielectric medium (dual superconductor) with vanishing chromoelectric permeability and infinite magnetic permeability. Glueballs are floating bubbles in the physical vacuum (Fig.11) and their perturbative interior is occupied by constituent TE and TM gluon modes appropriate for the confining boundary conditions of a dual superconductor [35,36]. The energy density in the physi-

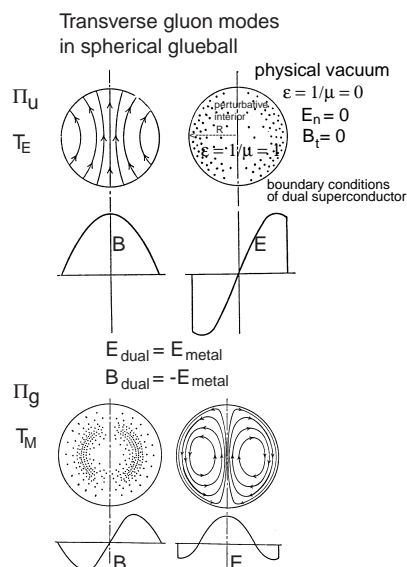


Figure 11. Hartree states of TE and TM gluon modes.

cal vacuum (which is the required vacuum energy to create the bubble) is given by the well-known expression  $B = -\frac{9}{32\pi}\alpha_s\langle 0|F_{\mu\nu}^2|0\rangle$  from the trace anomaly of the energy-momentum tensor [37]. The quantum numbers and energies of the lowest gluon modes are given in Table 2 and the fields of the TE and TM modes are depicted in Fig.11. The energy of the localized glueball is calculated

Table 2

Lowest TE and TM gluon modes in spherical bubble with energies  $x_i/R$  for the  $i^{\text{th}}$  mode.

l	mode	$J^P$	$x_i$
1	TE	$1^+$	2.744
2	TE	$2^-$	3.96
1	TM	$1^-$	4.49

from

$$E_{\text{glueball}} = \frac{4\pi}{3}R^3B + \sum_i n_i x_i/R - c \frac{\alpha_s}{R} \lambda_1^a \lambda_2^a \vec{S}_1 \vec{S}_2, \quad (1)$$

where  $n_i$  is the occupation number of the  $i^{\text{th}}$  gluon mode and the numerical constant  $c$  is close to  $1/4$ . The last term in Eq. (1) represents the interaction energy of the gluon modes. I chose  $B^{1/4} = 280$  MeV for the vacuum energy density which is appropriate for heavy quark spectroscopy and the hybrid potentials [38] ( $B^{1/4} \sim 250$  MeV – 350 MeV is the preferred range from the evaluation of the gluon condensate [37]). The mass of the glueball has to be corrected for the localization of the center-of-mass,

$$M_{\text{glueball}}^2 = E_{\text{glueball}}^2 - \sum_i n_i x_i^2/R^2, \quad (2)$$

where the second term is an estimate of the kinetic energy  $\langle \vec{P}^2 \rangle$ . The energies and radii of the various glueball states are determined from the minimization of Eqs.(1,2) with respect to  $R$ . The spectrum is displayed in Fig.10 with  $\alpha_s(1/R) = 0.5$  where  $R \approx 0.5$  fm.

The old bag calculations of the glueball spectrum did not work. They led to very low glueball masses with wrong spin splittings for two reasons: the wrong value of  $B$  and an unacceptably large effective  $\alpha_s$  were used simultaneously from light hadron spectroscopy [35,36]. I have

nothing to say about light hadrons which are intimately connected with the chiral condensate of the vacuum. In contrast, the dual superconductor picture gives consistent phenomenology for so many aspects of the microscopic vacuum structure in the gluon sector of the theory [38]. It remains a mystery why this simple caricature of glueball states works so well in describing the quenched spectrum. Only a microscopic theory of the vacuum could shed light on this question.

### 3. THE CONFINING FLUX

I will discuss first an interesting microscopic vacuum model to illustrate the generic features of the confining flux. The Lagrangian of the same model was also used in two contributions to the conference in the study of flux fission (string breaking) [39,40].

#### Microscopic Vacuum Model

We will investigate the response of the microscopic monopole vacuum to Wilson loops in the 2+1 dimensional Georgi-Glashow model as the simplest example of quark confinement [41]. In the Higg vacuum of the theory the SU(2) gauge symmetry is broken to U(1) with a neutral and massless gauge boson  $A_\mu$ . The massive Higgs boson is frozen out from the low energy theory, together, in the weak coupling limit  $g^2/m_W \ll 1$ , with the two massive gauge bosons  $W^\pm$  where the dimensional gauge coupling  $g$  sets the physical scale. The euclidean vacuum is dominated by a dilute gas of instantons which are 't Hooft-Polyakov monopoles interacting with a magnetic Coulomb force.

The monopole vacuum responds to external U(1) charges by flux formation. This is calculable from the response of the vacuum to an external magnetic potential  $\eta$ , given by the partition function

$$Z(\eta) = \int \mathcal{D}\chi \exp \left\{ -\frac{g^2}{16\pi^2} \int \left[ \frac{1}{2} (\nabla(\chi - \frac{1}{2}\eta))^2 - M^2 \cos\chi \right] d^3r \right\}, \quad (3)$$

in the sine-Gordon field representation of the monopole plasma [41]. The sine-Gordon mass

$M$  is expressed in terms of the fugacity  $\zeta$  of the monopole plasma by  $M^2 = 32\pi^2\zeta/g^2$  where  $\zeta \sim \exp(-\text{const} \cdot m_W/g^2)$  is exponentially small in the weak coupling limit so that we have a dilute monopole system. A pair of static sources corresponds to an external magnetic potential  $\eta_{wl}$  which is generated by an imaginary current  $I = i \cdot g/2$  running around the Wilson loop immersed in the monopole plasma,  $\langle \exp(i \int A_\mu dx_\mu) \rangle = Z(\eta_{wl})/Z(0)$ . In the weak coupling limit the semiclassical expansion is applicable (Debye-Hückel theory), and flux formation in leading order is described by the solution of the sine-Gordon equation in the presence of the current loop. An exact sine-Gordon soliton solution at infinite separation of the sources,

$$\chi_{\text{soliton}} = \begin{cases} 4\text{arctg}(\exp(-My)) & , y > 0 \\ -4\text{arctg}(\exp(+My)) & , y < 0 \end{cases} \quad (4)$$

describes a confining flux running along the  $x$  direction, with the transverse profile given by  $\chi_{\text{soliton}}$  in the  $y$ -direction. This solution in 2+1 dimensional Minkowski space-time corresponds to the electric flux profile

$$\vec{E}_{\text{Minkowski}} = \left( -\frac{gM}{2\pi} \frac{1}{\cosh(My)}, 0 \right)$$

where the width of the flux which contains more than 90 percent of the flux energy is approximately  $4M$ , set by the Debye-Hückel (sine-Gordon) mass  $M$ . The asymptotic value of the string tension is given by  $\sigma = \frac{g^2}{2\pi^2} M$ .

At finite separation of the sources we solve the sine-Gordon equation numerically [42] with typical solutions depicted in Fig.12. We find a growing and stretching bubble in the vacuum crossing from oblate to prolate shape and asymptotically converging to the shape and intrinsic profile of the exact solution of Eq. (4) between the two fixed sources but not close to them. The vortex energy is shown in Fig.13. When the separation of the sources becomes comparable to the width of the flux, the rapid onset of linear behavior in the flux energy, well before the asymptotic form of the flux is reached, is a remarkable feature of Figs.12,13. It is likely that a rather similar situation occurs in QCD where we would like to answer the question: What sets the scale of string formation?



Flux formation in monopole vacuum

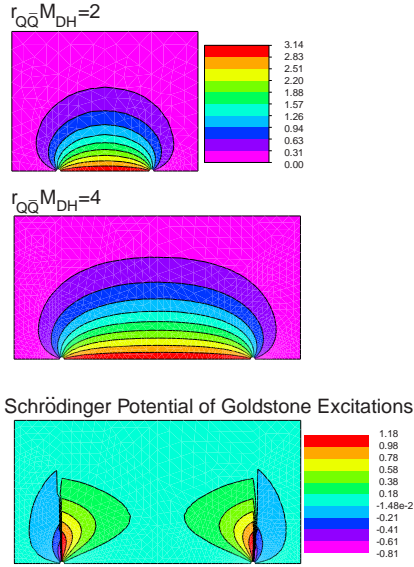


Figure 12. Flux profiles at small and intermediate separation of the sources. The bottom part is a contour plot of distortions on the gutter shaped effective Schrödinger potential as discussed in the text.

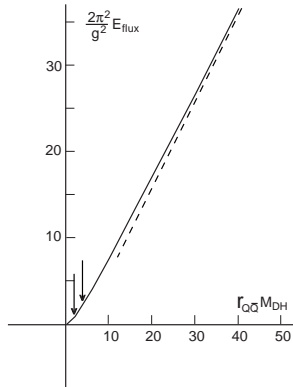


Figure 13. Flux energy with arrows indicating the flux configurations of Fig.12. The slope of the dashed line is the exact string tension of the infinitely long flux.

### Casimir Scaling and Multiple Sources

Several interesting tests can be done in QCD on the flux formation mechanism without looking

into the details of the excitation spectrum. One can excite the color sources at the two ends by putting the quark and the antiquark into higher representations of the  $SU(3)$  color group, or investigate flux formation with several quark sources.

Casimir scaling was a much discussed topic at the conference: according to folklore the string tension should be proportional to the value of the Casimir operator in the color group representation. Deldar reported results for the flux energy in the sextet and octet color representations of the static quark-antiquark pair [43]. A linearly rising potential with Casimir scaling was observed in the approximate range of 0.5 fm to 1.2 fm source separation, even for octet sources where gluon screening is expected to split the flux asymptotically. This is in agreement with earlier findings [45,44].

Although it is popular to interpret Casimir scaling at intermediate  $Q\bar{Q}$ -separation as a test of microscopic confinement mechanisms ( $Z(N)$  flux, monopoles, etc.), the test remains incomplete without a more detailed microscopic understanding of flux formation and its dependence on color representations [46].

In some interesting work in progress [21], the potential energy of the 3Q system was studied. Anticipating the formation of a Y-shape string at large separation, the potential is plotted in Fig.14 as a function of inter-quark separation when the three quark sources are located in a plane at equal angles. The lesson from the growing and stretch-

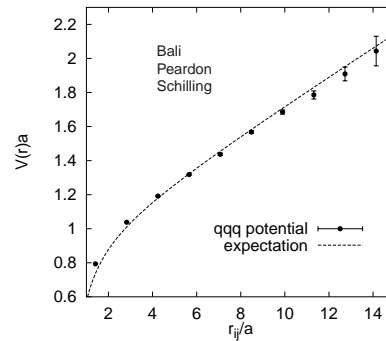


Figure 14. 3Q potential in Y-configuration.

ing bubble is that the rapid onset of the linear potential cannot be interpreted as evidence for the early formation of a Y-shape string. Earlier work in the bag model illustrates that a very similar potential energy shape develops precociously before string formation [5], as depicted in Fig.15.

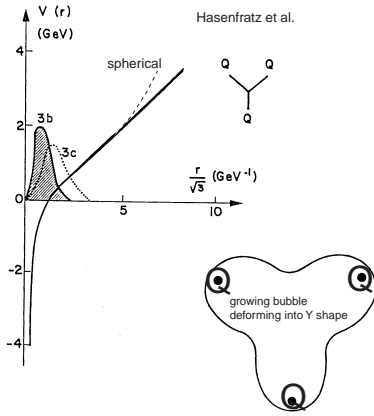


Figure 15. 3Q bag potential in Y-configuration. The dashed line indicates spherical approximation.

Interesting new results were also reported at the conference on 4Q flux configurations [48] which hopefully will advance our understanding of flux formation in the confining vacuum.

### Where Is the String Limit?

The confining flux is represented by the quantum sine-Gordon soliton in the monopole vacuum. Excitations of the flux are given by the spectrum of the fluctuation operator  $\mathcal{M} = -\nabla^2 + U''(\chi_{\text{soliton}})$  where  $U(\chi)$  is the field potential energy of the sine-Gordon field. The spectrum of the fluctuation operator  $\mathcal{M}$  is determined from a two-dimensional Schrödinger equation at finite separation of the sources. In the limit of asymptotically large  $r_{Q\bar{Q}}$ , the equation becomes separable in the longitudinal  $x$  and transverse  $y$  coordinates. The transverse spectrum is in close analogy with the quantization of the one-dimensional classical sine-Gordon soliton. There is always a discrete zero mode in the spectrum

which is enforced by translational invariance in the transverse direction. Scattering states of massive gauge bosons (“glueballs”) on the confining flux are separated by the mass gap  $M$  of the sine-Gordon theory.

Plane wave excitations with momentum  $k$  along the longitudinal direction, when combined with the zero mode of the transverse spectrum, correspond to Goldstone excitations along the infinitely long flux. This spectrum is mapped into the spectrum of a string in the semiclassical quantization procedure [49]. In string theory, the string with fixed ends is described by Dirichlet boundary conditions which would correspond to closing down on the two ends the long effective Schrödinger potential well with two infinite potential walls (a gutter between infinite walls).

At finite  $r_{Q\bar{Q}}$ , this picture, however is grossly distorted. Far from the sources and from the main axis, the effective Schrödinger potential well always has a finite height  $M$ . Therefore the gutter should be closed by two walls of finite height  $M$  which are penetrable and distort the Goldstone spectrum. In addition, as depicted in Fig.12, the potential well is further deformed close to the sources. As a consequence, at smaller separation of the sources, the fluctuation spectrum is not string-like at all. At large separations, however, the fluctuation spectrum of the quantum soliton (confining flux) will smoothly deform with growing  $r_{Q\bar{Q}}$  into the expected Goldstone spectrum. Based on the above picture this is not expected before the length of the flux exceeds several times the width of the flux.

In QCD the robust features of the Goldstone spectrum of the confining flux are described by an effective string theory where the two-dimensional vector  $\vec{\xi}$  measures the deviations of the flux from its straight line position [50]. The effective low energy expansion is based on the assumption that massive intrinsic excitations of the flux are decoupled at low energies from the low-energy string-like excitations. The effective Lagrangian of this description has two important symmetries: Euclidean invariance in the world sheet variables and  $O(2)$  translations and rotations in the  $\vec{\xi}$  field variable. The second symmetry requires that  $\mathcal{L}_{\text{eff}}(\vec{\xi})$  can only depend on the derivatives of  $\vec{\xi}$ ,

$\mathcal{L}_{\text{eff}} = \frac{1}{2}\alpha\partial_\mu\vec{\xi}\cdot\partial_\mu\vec{\xi} + \dots$ , where the dots represent terms with four, or more derivatives and  $\alpha$  is a dimensional constant. For low frequency excitations the first term in  $\mathcal{L}_{\text{eff}}(\vec{\xi})$  dominates all the higher dimensional operators.

The Gaussian effective Lagrangian of the fluctuating flux describes massless Goldstone excitations which are associated with the restoration of Euclidean translations and rotations due to the formation of the confining quantum flux. The full non-linear realization of euclidean symmetries on  $\vec{\xi}$  would amount to the summation of higher derivative operators requiring special coefficients and resulting in the Nambu-Goto action,

$$\mathcal{L}_{\text{eff}} = \alpha\sqrt{1 + \partial_\mu\vec{\xi}\cdot\partial_\mu\vec{\xi}} = \frac{1}{2}\alpha\partial_\mu\vec{\xi}\cdot\partial_\mu\vec{\xi} + \dots \quad (5)$$

This is in analogy with the nonlinear chiral Lagrangian of massless pions. However, the special higher derivative terms in the expansion of the Nambu-Goto action will compete with other higher dimensional operators (rigidity, torsion, and some other properties of the confining flux). It is, therefore, difficult to believe that the Nambu-Goto action would play any useful role in the description of the excitation spectrum of the confining flux.

The ground state energy of a string of length  $L$  with clamped ends is given by

$$E_0(L) = \sigma \cdot L - \frac{\pi}{12L} + \dots \quad (6)$$

in 1-loop approximation where  $\sigma$  designates the string tension and the second term represents the Casimir energy of zero-point fluctuations [50]. The excitation energies above the ground state have the simple string spectrum,

$$E_n = E_0 + n \cdot \frac{\pi}{L}, \quad n = 1, 2, 3, \dots \quad (7)$$

It was repeatedly claimed by lattice practitioners that the Casimir term was seen in the static quark-antiquark potential (string ground state) for less than two fermi separation, interpreted as strong evidence for string formation in QCD. I will show now that this claim was intrinsically flawed.

In QCD we do not have the underlying microscopic theoretical picture of the confining vac-

uum, but we expect to learn about it by the determination of the excitation spectrum of the confining flux in lattice simulations. The first step in determining the spectrum of the stationary states of the gluon field in the presence of the static quark-antiquark pair, fixed in space some distance  $r_{Q\bar{Q}}$  apart, is to classify the energy levels in terms of the symmetries of the problem [13]. Such a system has cylindrical symmetry about the axis  $\hat{\mathbf{r}}$  passing through the static quark and the antiquark (the molecular axis). The total angular momentum of the gluons is not a conserved quantity, but its projection onto the molecular axis is and can be used to label the energy levels of the gluon field. We adopt the standard notation from the physics of diatomic molecules and use  $\Lambda$  to denote the magnitude of the eigenvalue of the projection  $\vec{J}_g \cdot \hat{\mathbf{r}}$  of the total angular momentum  $\vec{J}_g$  of the gluon field onto the molecular axis  $\hat{\mathbf{r}}$ . The capital Greek letters  $\Sigma, \Pi, \Delta, \Phi, \dots$  are used to indicate states with  $\Lambda = 0, 1, 2, 3, \dots$ , respectively. The energy of the gluon field is unaffected by reflections in a plane containing the molecular axis; since such reflections interchange states of opposite handedness, given by the sign of  $\vec{J}_g \cdot \hat{\mathbf{r}}$ , such states must necessarily be degenerate ( $\Lambda$  doubling). However, this doubling does not apply to the  $\Sigma$  states;  $\Sigma$  states which are even (odd) under a reflection in a plane containing the molecular axis are denoted by a superscript  $+$  ( $-$ ). The combined operations of charge conjugation and spatial inversion about the midpoint between the quark and the antiquark is also a symmetry and its eigenvalue is denoted by  $\eta_{CP}$ . States with  $\eta_{CP} = 1(-1)$  are denoted by the subscripts  $g$  ( $u$ ). Hence, the low-lying levels are labelled  $\Sigma_g^+, \Sigma_g^-, \Sigma_u^+, \Sigma_u^-, \Pi_g, \Pi_u, \Delta_g, \Delta_u$ , and so on. For convenience, we use  $\Gamma$  to denote these labels in general.

The continuum-limit extrapolations [13] are shown in Fig.16. The ground state  $\Sigma_g^+$  is the familiar static-quark potential. A linearly-rising behaviour dominates the  $\Sigma_g^+$  potential once  $r$  exceeds about 0.5 fm and we find no deviations from the linear form up to 4 fm. The lowest-lying excitation is the  $\Pi_u$ . There is definite evidence of a band structure at large separation: the  $\Sigma_g^{+'}, \Pi_g,$

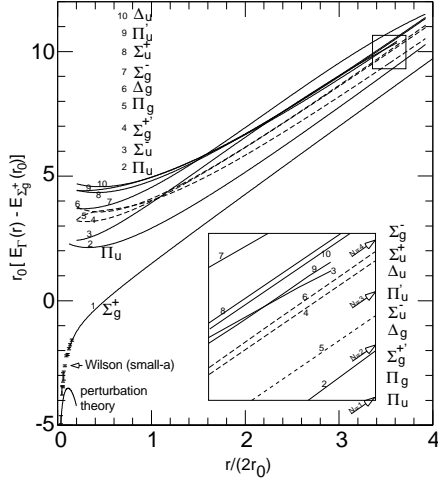


Figure 16. The excitation spectrum of the confining flux. The energy levels of  $N=1,2,3,4$  Goldstone excitations are shown in the insert.

and  $\Delta_g$  form the first band above the  $\Pi_u$ ; the  $\Sigma_u^+$ ,  $\Sigma_u^-$ ,  $\Pi_u'/\Phi_u$ , and  $\Delta_u$  form another band. The  $\Sigma_g^-$  is the highest level at large  $r_{Q\bar{Q}}$ . This band structure breaks down as the separation of the sources decreases below 2 fm. In particular, two levels, the  $\Sigma_g^-$  and  $\Sigma_u^-$ , drop far below their degenerate partners as the separation between sources becomes small. Note that for  $r_{Q\bar{Q}}$  above 0.5 fm, all of the excitations shown are stable with respect to glueball decay. As the separation of the sources decreases below 0.5 fm, the excited levels eventually become unstable as their gaps above the ground state  $\Sigma_g^+$  exceed the mass of the lightest glueball.

The level orderings and approximate degeneracies of the gluon energies at large separation match those expected of the Goldstone modes. However, the precise Goldstone gap behaviour is not observed. The two  $\Sigma^-$  states are in violent disagreement with expectations from a fluctuating string. Note also that the results clearly disagree with the energy spectrum of a Nambu-Goto string naively applied in four continuous space-time dimensions.

These results are rather surprising and cast serious doubts on the validity of treating glue in terms of a fluctuating string for quark-antiquark

separations less than 2 fm. Note that such a conclusion does not contradict the fact that the  $\Sigma_g^+$  ground state energy rises linearly for  $r_{Q\bar{Q}}$  as small as 0.5 fm. A linearly-rising term is not necessarily indicative of a string as we have seen in earlier examples. For  $r_{Q\bar{Q}}$  greater than 2 fm, there are some tantalizing signatures of Goldstone mode formation, yet significant disagreements still remain. To what degree these discrepancies can be explained in terms of distortions of the Goldstone mode spectrum arising from the spatial fixation of the quark and antiquark sources (clamping effect) is currently under investigation [42].

For reasons explained here I remain puzzled and reserved on reported results that large Wilson loops in lower dimensional models agree with the predictions of a fluctuating string [57] even for relatively small separation of the sources.

### Flux Fission (String Breaking)

The confining flux is expected to fission into a pair of static mesons, also known as string breaking, when its energy is large enough to pair produce light dynamical quarks. At large separation of the color sources the static potential, as calculated from Wilson loops, describes the force between static mesons which are color sources screened by light quark fields (like the static B meson in the infinite b-quark mass limit). We expect the linearly rising potential to asymptotically cross over into Yukawa form controlled by the lowest mass exchange (pion). The attractive, or repulsive nature of the Yukawa force will depend on the spin-isospin quantum numbers of the static  $B\bar{B}$  pair which is not taken into account in Wilson loop operators. The crossover range is expected to occur at a separation where the energy of the confining flux exceeds twice the static meson energy.

In QCD simulations with two flavors of dynamical quarks, where the crossover range has been reached, new results were reported at the conference (Fig.17) without any visible string breaking effects [1,51,52]. It was suggested using strong coupling ideas [53] that string breaking is a mixing phenomenon, involving both the string and the static two-meson state. Thus, in order to confirm the mixing picture, the conven-

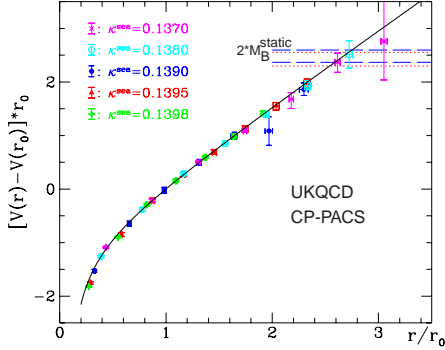


Figure 17. Dynamical fermion loop effects on the static potential.

tionally used Wilson loops have to be supplemented by explicit two-meson operators. This idea was illustrated in two contributions to the conference [39,40] studying the Georgi-Glashow model with the Higgs field in the fundamental representation playing the role of the screening matter field. In Fig.18 results from the three-dimensional model are shown [39] with findings very similar to the four-dimensional study [40]. Since the quenched static potential between ad-

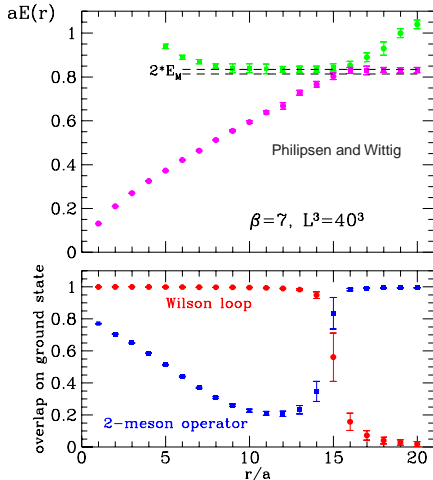


Figure 18. Mixing effects between the Wilson loop operator and two static mesons.

joint sources is screened by the gluon field, its study would also provide further tests on string

breaking [44,45].

It was reported at the conference from the study of Polyakov loop correlators, where mixing with the static meson pair is different from Wilson loops, that the finite temperature static potential does exhibit screening behavior [54]. Since the calculation was done just below the deconfining temperature it would be interesting to extend this work to lower temperatures. It was also reported that the screening of large Wilson loops was easy to detect in lower dimensional models [55,56].

## Acknowledgements

I would like to thank G. Bali, R. Burkhalter, R. Kenway, P. Lacock, C. Morningstar, M. Pardon, and D. Toussaint for help in the preparation of this talk. I am also thankful to the organizers of the conference who created a stimulating atmosphere throughout the meeting. This work was supported by the U.S. DOE, Grant No. DE-FG03-97ER40546.

## REFERENCES

1. R. Kenway, this Proceedings.
2. P. Lacock and K. Schilling (SESAM Collaboration), this proceedings, hep-lat/9809022.
3. J. W. Negele, A. Pochinsky, B. Scarlet, this proceedings, hep-lat/9809077.
4. W. Lee and D. Weingarten, hep-lat/9805029; D. Weingarten, this Proceedings.
5. P. Hasenfratz, R. Horgan, J. Kuti, J. Richard, Phys. Lett., B95 (1980) 299.
6. D. Horn and J. Mandula, Phys. Rev., D17 (1978) 898.
7. B. A. Thacker and G. P. Lepage, Phys. Rev., D43 (1991) 196.
8. C. Bernard et al., this proceedings, hep-lat/9809087.
9. D.M.J. Lovelock et al., Phys. Rev. Lett., 54 (1985) 377.
10. D. Besson et al., Phys. Rev. Lett., 54 (1985) 381.
11. E. Eichten, Phys. Rev., D22 (1980) 1819.
12. K.J. Juge, J. Kuti, and C. Morningstar, Nucl. Phys. Proc. Suppl., 63 (1998) 326.

13. K.J. Juge, J. Kuti, and C. Morningstar, this proceedings, hep-lat/9809098.
14. G. Bali, private communication, to be published.
15. S. Perantonis and C. Michael, Nucl. Phys., B347 (1990) 854.
16. R. Sommer, Nucl. Phys., B411 (1994) 839.
17. G. Bali, private communication, to be published.
18. T. Manke, I.T. Drummond, R.R. Horgan, and H.P. Shanahan, Phys. Rev., D57 (1998) 3829.
19. S. Collins, Nucl. Phys. Proc. Suppl., 63 (1998) 335.
20. Bernard et al., Phys. Rev., D56 (1997) 7039.
21. G.S. Bali, K. Schilling, and A. Wachter, Phys. Rev., D56 (1997) 2566.
22. C. Morningstar and M. Peardon, Phys. Rev., D56 (1977) 4043.
23. M. Peardon, Nucl. Phys. Proc. Suppl., 63 (1998) 22-27.
24. C. Morningstar and M. Peardon, paper in preparation.
25. N.H. Shakespeare, H.D. Trottier, this proceedings, hep-lat/9803024.
26. UKQCD Collaboration, Phys. Lett., B309 (1993), 378.
27. V. Anisovich et al., Phys. Lett., B323 (1994) 233.
28. R.M. Baltrusaitis et al., Phys. Rev. Lett., 56 (1986) 107.
29. R. Godang et al., Phys. Rev. Lett., 79 (1997) 3829
30. J. Sexton, A. Vaccarino, D. Weingarten, Phys. Rev. Lett., 75 (1995) 4563.
31. G.S. Bali et al., Nucl. Phys. Proc. Suppl., 63 (1998) 209.
32. H. Fritzsche, P. Minkowski, Nuovo Cim., 30A (1975) 393.
33. J. Bjorken, 1979 SLAC Summer Institute, SLAC-PUB-2372 (1979).
34. R.L. Jaffe, K. Johnson, Z. Ryzak, Annals of Phys., 168 (1986) 344.
35. T. Barnes, F.E. Close, S. Monaghan, Nucl. Phys., B198 (1982) 380.
36. C.E. Carlson, T.H. Hansson, C. Peterson, Phys. Rev., D27 (1983) 1556. Nucl. Phys., B198 (1982) 380.
37. M.A. Shifman (editor), *Vacuum structure and QCD sum rules*, North-Holland publisher (1992).
38. K.J. Juge, J. Kuti, and C. Morningstar, Nucl. Phys. Proc. Suppl., 63 (1998) 543.
39. O. Philipsen, H. Wittig, this proceedings, hep-lat/9809093.
40. F. Knechtli, this proceedings, hep-lat/9809021.
41. A.M. Polyakov, Nucl. Phys., B120 (1977) 429.
42. K.J. Juge, J. Kuti, and C. Morningstar, in preparation.
43. S. Deldar, this proceedings, hep-lat/9809137.
44. N.A. Campbell, I.H. Jorysz, C. Michael Phys. Lett., 167B (1986) 91.
45. G.I. Poulis, H.D. Trottier, Phys. Lett., B400 (1997) 358.
46. J. Greensite, this proceedings, hep-lat/9809053.
47. G. Bali, M. Peardon, K. Schilling, work in preparation.
48. P. Pennanen, this proceedings, hep-lat/9809035.
49. M. Lüscher, K. Symanzik, P. Weisz, Nucl. Phys., B173 (1980) 365.
50. M. Lüscher, Nucl. Phys., B180 (1981) 317.
51. M. Talevi (UKQCD collaboration), this proceedings, hep-lat/9809182.
52. S. Aoki et al. (CP-PACS collaboration), this proceedings, hep-lat/9809185.
53. I.T. Drummond, this proceedings, hep-lat/9807038.
54. E. Laermann, C. DeTar, O. Kaczmarek, F. Karsch, this proceedings, hep-lat/9809105.
55. A. Duncan, E. Eichten, H. Thacker, this proceedings, hep-lat/9809144
56. H.D. Trottier, this proceedings, hep-lat/9809183.
57. M. Caselle, R. Fiore, F. Gliozzi, Nucl. Phys., B486 (1997) 245.